AIP Advances

Analysis and equivalent circuit for accurate wideband calculations of the impedance for a piezoelectric transducer having loss

Cite as: AIP Advances **9**, 085313 (2019); https://doi.org/10.1063/1.5118897
Submitted: 05 July 2019 . Accepted: 07 August 2019 . Published Online: 19 August 2019

M. J. Hagmann

View Online Export Citation CrossMark

ARTICLES YOU MAY BE INTERESTED IN

Parasitic analysis and π-type Butterworth-Van Dyke model for complementary-metal-oxide-semiconductor Lamb wave resonator with accurate two-port Y-parameter characterizations
Review of Scientific Instruments **87**, 045004 (2016); https://doi.org/10.1063/1.4945801

1D thermal characterization of micro/nano-cantilevers for Suspended ThermoReflectance measurements
AIP Advances **9**, 085315 (2019); https://doi.org/10.1063/1.5115512

Temperature-dependent phonon dynamics of supported and suspended monolayer tungsten diselenide
AIP Advances **9**, 085316 (2019); https://doi.org/10.1063/1.5118004

NEW!
Sign up for topic alerts
New articles delivered to your inbox
AIP Publishing

AIP Publishing

© 2019 Author(s).

Analysis and equivalent circuit for accurate wideband calculations of the impedance for a piezoelectric transducer having loss

Cite as: AIP Advances 9, 085313 (2019); doi: 10.1063/1.5118897
Submitted: 5 July 2019 • Accepted: 7 August 2019 •
Published Online: 19 August 2019

View Online Export Citation CrossMark

M. J. Hagmann[a)]

AFFILIATIONS

NewPath Research L.L.C., Salt Lake City, Utah 84115, USA

[a)]Email: mhagmann@newpathresearch.com

ABSTRACT

Others have analyzed the operation of piezoelectric transducers by defining two complex parameters which have the units of frequency to allow for the effects of loss. The present paper presents an analysis in which this procedure is extended to include harmonics as well as the fundamental frequency. In this extension it is seen that both positive and negative extrema in both the resistance and the conductance occur at a series of harmonics. Equivalent circuits are also presented with examples for both high-Q and low-Q materials showing agreement with these simulations.

© 2019 Author(s). All article content, except where otherwise noted, is licensed under a Creative Commons Attribution (CC BY) license (http://creativecommons.org/licenses/by/4.0/). https://doi.org/10.1063/1.5118897

I. INTRODUCTION

Berlincourt *et al.*[1] and Meeker[2] derived expressions for the electrical impedance of a piezoelectric disk transducer in the thickness modes when the loss is negligible. Sherrit *et al.*[3] wrote this equation in the following form, and Sherrit and Mukerjee[4] presented other equations having a similar form for modes with other types of piezoelectric transducers.

$$Z(\omega) = \frac{t}{jA\omega\varepsilon_{33}^{S}}\left[1 - \frac{4k_t{}^2F_p}{\omega}\tan\left(\frac{\omega}{4F_p}\right)\right] \quad (1)$$

Here ω is the angular frequency, and the relevant material constants and calculated parameters for Eq. (1) that were defined and evaluated for the first two examples by Sherrit *et al.*[3] are given in Tables I and II. For clarity we use the symbol F_p which is defined in Table II instead of f_p, where the symbols f_p and f_s are defined and used later in the present derivation.

Berlincourt *et al.*[1] and Meeker[2] assumed zero loss so they used real values for all of the material parameters which requires that the impedance is purely reactive with singularities at frequencies that are odd integer multiples of F_p. However, Sherrit *et al.*[3] used measured values for the material parameters and dimensions that are complex to include the effects of loss and are given in Table I which we have used in examples. Table II shows the corresponding calculated parameters.

II. ANALYSIS SHOWING THE RESONANCES

Equation (1) may be written as the difference of two separate terms. The first, which is referred to as the "baseline impedance", varies inversely with the frequency while the second term has a series of resonances that are superimposed on the baseline impedance. The ratio of the second term to the baseline impedance is given by the following expression:

$$\text{Ratio}(\omega) = -\frac{4k_t{}^2F_p}{\omega}\tan\left(\frac{\omega}{4F_p}\right) \quad (2)$$

Figure 1 shows the magnitude of this ratio for the first 13 resonances (n = 1, 3, 5, . . ., 25) calculated using the material constants and calculated parameters for the high-Q and low-Q examples in Tables I and II. Note that the ratio decreases monotonically with the multiplier and the low-Q example has no peak beyond the 10th harmonic. In narrowband applications, such as with a piezoelectric resonator, it may be sufficient to consider only the first resonance. However, now we generalize and extend the equivalent circuit model

© Author(s) 2019

TABLE I. Material constants.

Parameter	Description	High-Q (Q = 100)	Low-Q (Q = 10)
e_{33}	Piezoelectric coeff. C/m^2	15.8/-0.860°	15.8/-0.860°
$c_{33}{}^D$	Elastic stiffness, N/m^2	1.47x10^{11}/0.571°	1.47x10^{11}/5.71°
$\varepsilon_{33}{}^S$	Clamped permittivity, F/m	7.35x10^{-9}/-1.15°	7.35x10^{-9}/-1.15°
ρ	Density, kg/m^3	7.70x10^3	7.70x10^3
t	Disk thickness, m	2.00x10^{-3}	2.00x10^{-3}
d	Disk diameter, m	2.54x10^{-2}	2.54x10^{-2}

TABLE II. Calculated parameters.

Parameter	Expression	High-Q (Q = 100)	Low-Q (Q= 10)
Piezoelectric field constant, V/m	$h_{33} = \frac{e_{33}}{\varepsilon_{33}{}^S}$	2.15x10^9/0.290°	2.15x10^9/0.290°
Electromechanical coupling constant	$k_t{}^2 = \frac{h_{33}{}^2 \varepsilon_{33}{}^S}{c_{33}{}^D}$	0.231/-1.15°	0.230/-6.28°
Parallel resonance frequency, Hz	$F_p = \frac{1}{2t}\sqrt{\frac{c_{33}{}^D}{\rho}}$	1.09x10^6/0.290°	1.10x10^6/2.86°

to a much greater bandwidth than the single resonance studied by Sherrit *et al.*[3]

The IEEE/ANSI standard on piezoelectricity[5] defines two parameters, f_p and f_s, as the real values for the frequencies at maximum resistance and maximum conductance, respectively. These two parameters are using Eq. (1) and its reciprocal for the admittance. These two parameters enable defining an equivalent circuit to provide the resonant frequencies for the cases of parallel and series excitation, respectively. We follow the extension of Eq. (1) which was made by Sherrit *et al.*[6] for the case of lossy materials for which f_p and f_s are complex numbers.

In searches of the complex frequency plane that we made using Eq. (1) and the corresponding equation for the admittance we have found a sequence of sharply-defined maxima for both the real part of the impedance Re[Z], and the real part of the admittance Re[Y].

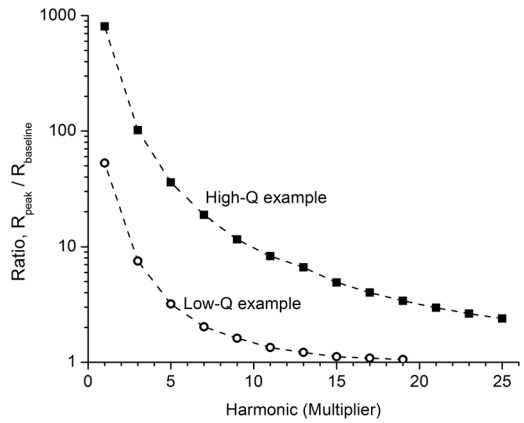

FIG. 1. Ratio of resistance at the peak in the second term of Eq. (1) to that in. the first term (baseline) for the high-Q and low-Q examples in Tables I and II.

We define the complex parameters γ and α such that $f_p = \gamma F_p$ and $f_s = \alpha F_p$ respectively at the maxima for Re[Z] and Re[Y] where F_p was defined in Table II.

A. Effect of parameter γ on the real part of the complex impedance

For the case of zero loss, at which Z is purely imaginary, there is a singularity when γ is an odd real integer. Thus, to provide continuity to the case of low loss, we examine the behavior of Eq. (1) for the impedance at $\gamma = n + \delta$ when n is an odd integer and δ is small and may be complex.

$$Z(\gamma) = \frac{t}{j2\pi A\gamma F_p \varepsilon_{33}^S}\left[1 - k_t{}^2\left(\frac{2}{\pi\gamma}\right)\tan\left(\frac{\pi\gamma}{2}\right)\right] \tag{3}$$

$$= \frac{t}{j2\pi A(n+\delta) F_p \varepsilon_{33}^S}\left[1 - \frac{2k_t{}^2}{\pi(n+\delta)}\tan\left(\frac{n\pi}{2} + \frac{\pi\delta}{2}\right)\right] \tag{4}$$

$$= \frac{t}{j2\pi A(n+\delta) F_p \varepsilon_{33}^S}\left[1 + \frac{2k_t{}^2}{\pi(n+\delta)}\cot\left(\frac{\pi\delta}{2}\right)\right] \tag{5}$$

$$\approx \frac{4k_t{}^2 t}{jA2\pi^3 n^2 F_p \varepsilon_{33}^S \delta} \tag{6}$$

Equation (6) shows that there is a singularity in the impedance which occurs as the modulus $|\delta| \rightarrow 0$ regardless of the argument of δ. This is consistent with our numerical simulations and confirms Sherrit's use of Fp as f_p when he only considered the first resonance.[3]

The singularity in the resistance R at the frequency $f = f_p$ requires that the susceptance B must be zero at this frequency. This may be seen by examining the relationship of the impedance to the admittance. For $Y = G + jB$, $Re[Z] = G/(G^2 + B^2)$ is bounded at all values of G when B is non-zero, but Re[Z] may be singular when B = 0.

© Author(s) 2019

Conversely, for Z = R +jX, then Re[Y] = R/(R^2 +X^2) is bounded for all values of R when X is non-zero, but Re[Y] may be singular when X = 0.

Figure 2 shows the real part of the complex impedance Z in the region of the complex frequency plane near the first resonance for the high-Q example in Tables I and II. The imaginary part of γ has the range of -10^{-9} to 10^{-9} with zero at the midpoint. The real part of γ has the range of 1-10^{-9} to 1+10^{-9} with 1 is at the midpoint. Figure 2 shows the neighborhood of the singularity near γ = 1 for the first resonance.

B. Effect of parameter α on the real part of the complex admittance

Our search of the complex frequency plane shows that near f_s, where Re[Y] has a maximum, the reactance Im[Z] is non-zero so that Re[Y] is not singular. Thus, we see large positive and negative values for Re[Y] when the complex frequency is near f_s but these values for Re[Y] are bounded.

Figure 3 shows the real part of the complex admittance in the region of the complex frequency plane near the first resonance for the high-Q example in Tables I and II. The center of the complex-Y plane in this figure is at $f_s = \alpha F_p$, where Re[α] = 0.8964968342 and Im[α] = 0.0022944067, where each of these parts is specified to 10 decimal places because the values of Y were determined at increments of 10^{-10} in both Re[α] and Im[α]. The imaginary part of α has a range of 0.0022944067-10^{-9} to 0.0022944067+10^{-9}, and the real part of α has a range of 0.8964968342 -10^{-9} to 0.8964968342 +10^{-9}. Figure 3 verifies that the susceptance Re[Y] has a sharp maximum but is non-singular.

In generating the data for Fig. 3, α was evaluated by maximizing Re[Y] based on Eq. (1), but now a simpler method for evaluating α will be presented. Equation (1) may be inverted to obtain the following expression for the admittance where trial values of α, labeled as

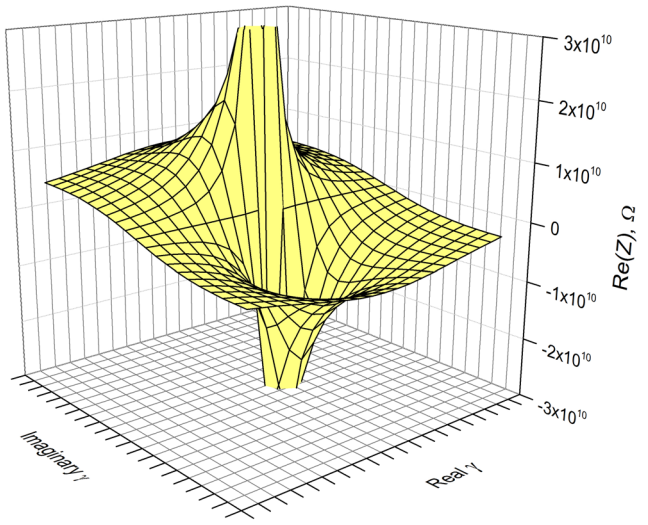

FIG. 2. Real part of the complex impedance as a function of the complex parameter γ at the first resonance for the high-Q example in Tables I and II.

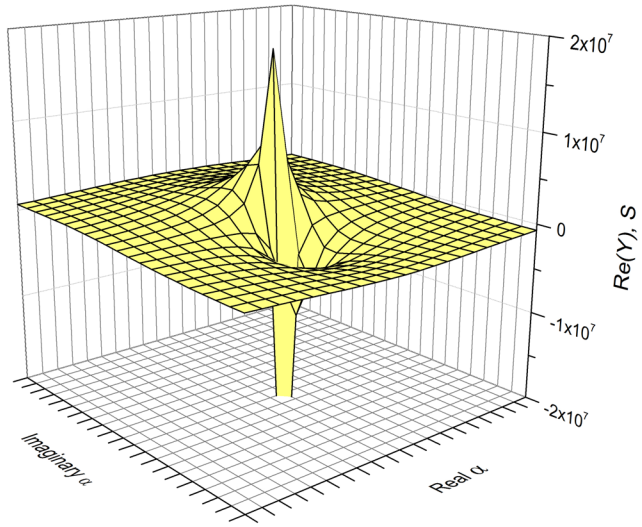

FIG. 3. Real part of the complex admittance as a function of the complex. parameter α at the first resonance for the high-Q example in Tables I and II.

α_t, may be used to maximize Re[Y(αt)] to determine α:

$$Y(\alpha_t) = \frac{j4AF_p\varepsilon_{33}^S}{t}\frac{\left(\frac{\pi\alpha_t}{2}\right)^2}{\left[\frac{\pi\alpha_t}{2} - k_t{}^2\tan\left(\frac{\pi\alpha_t}{2}\right)\right]} \tag{7}$$

It is not possible for the denominator in Eq. (7) to be exactly zero—for which Y would be singular. However, α may be approximated by minimizing $\left|\frac{\pi\alpha_t}{2} - k_t{}^2\tan\left(\frac{\pi\alpha_t}{2}\right)\right|$.

Figure 4 shows the imaginary part of α as a function of the harmonic (multiplier) minus the real part of α for the first five values of α. The harmonics are in decreasing order from left to right so the abscissa is 9 - α_R, for the high-Q and low-Q examples at the LHS and 1- α_R at the RHS. This figure shows that $\alpha_I \approx C(n - \alpha_R)$ for all of the harmonics for a particular piezoelectric resonator where C is a constant that depends on the properties of that device.

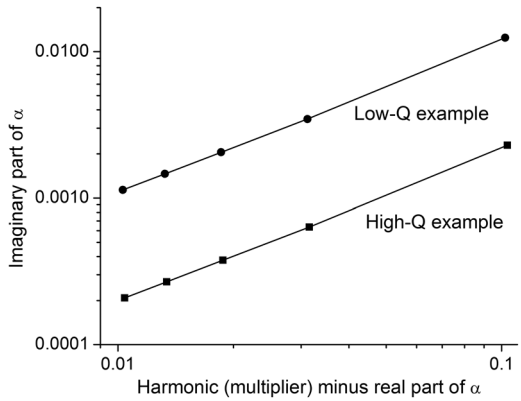

FIG. 4. Relationship of the imaginary and real parts of α determined for the high-Q and low-Q examples in Tables I and II.

© Author(s) 2019

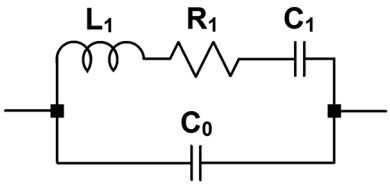

FIG. 5. Butterworth-Van Dyke model.

We have shown that accurate and efficient determination of α for multiple resonances with a single device is possible by using the technique described in the previous paragraph with the approximate relationship for the real and imaginary parts of α.

Sherrit et al.[7] have made the approximation of determining f_p and f_s by maximizing Re[fZ] and Re[Y/f] respectively. This simplifies the calculations but this procedure may be questioned because multiplying or dividing by the complex frequency causes a rotation in the complex plane. We have found that this approximation causes a small error which may generally be neglected, but all of the solutions for f_p and f_s in this paper were determined using Eq. (1) and its equivalent for admittance without further approximations.

III. EXTENSION OF THE SHERRIT EQUIVALENT CIRCUIT

The Butterworth-Van Dyke model for a piezoelectric resonator[8–10] has a resistor, inductor, and capacitor in series (R-L-C), all shunted by a second capacitor C_0 as shown in Fig. 5. Van Dyke was the first to propose this equivalent circuit, and he suggested extending the model by having multiple R-L-C circuits in parallel to include the effects of multiple resonances as shown in Fig. 6.[9] The Sherrit model is shown in Fig. 7[3] and our proposed extension of the Sherrit model for multiple resonances is shown in Fig. 8.

Table III gives the parameters for Butterworth-Van Dyke (BVD) and Sherrit equivalent circuits[3] for the high-Q and low-Q examples.

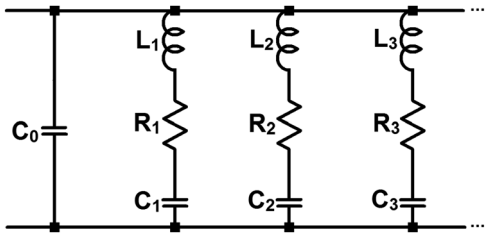

FIG. 6. Butterworth-Van Dyke extended model.

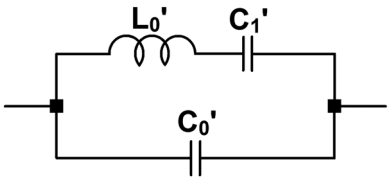

FIG. 7. Sherrit model.

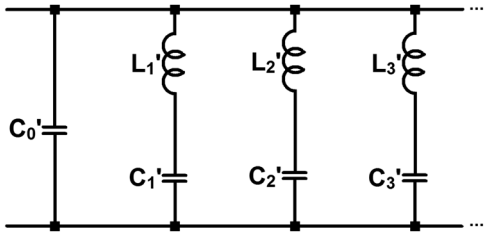

FIG. 8. Our proposed extension of the Sherrit model.

Figures 9 and 10 show the resistance and reactance simulated with these two equivalent circuits and with the analytical solution from Eq. (1). These calculations were only made for the high-Q example in Tables I and II. Figure 9 shows that the resistance for the Sherrit equivalent circuit is consistent with the analytical solution with the exception of missing the higher-order resonances. However, while the BVD model is accurate near the first resonance the resistance is too small above and below the resonance. This may be understood because well below the single resonance the resistance remains approximately constant since the current is divided by C_0 and C_1, and the only loss is in the resistor R_1 which is in series with C_1. The BVD model is also inaccurate well above resonance where the inductor L_1 causes a greater fraction of the current to flow through capacitor C_0 instead of through resistor R_1.

Figure 10 shows that the reactance calculated for the BVD and Sherrit equivalent circuits is in good agreement with that from Eq. (1), with the exception of the higher-order resonances that are seen in the analytical solution. This may be understood because well below the single resonance the reactance is approximately that for C_0 and C_1 or C_0' and C_1' in parallel, and well above the resonance the inductor causes the reactance to approximate that of C_0, or C_0', and the resonance is quite sharp for the high-Q example. Figures 9 and 10, are log-log plots to clarify that the resistive component of the impedance has two components as was previously stated; a baseline impedance varying inversely with the frequency as well as superimposed resonances.

We acknowledge that others have also used single and multi-branch equivalent circuits,[11,12] but Sherrit *et al.*[3] derived complex functions for the circuit elements from Eq. (1), and simulations using their equivalent circuit are consistent with Eq. (1) except for neglecting the higher-order resonances. The introduction of complex expressions for the circuit elements correctly associates the different types of loss with each circuit element. The following discussion considers our proposed extension of the Sherrit model which is shown in Fig. 8.

We begin by requiring that at low-frequencies the impedance of the equivalent circuit must agree with Eq. (1), so that now we must require the following:

$$Z(\omega) = \frac{t\left(1-k_t{}^2\right)}{jA\omega\varepsilon_{33}^S} = \frac{1}{j\omega(C_0{}' + C_1{}' + \cdots + C_N{}')} \tag{8}$$

where N is the number of branches in the equivalent circuit. Thus, once the capacitance in each branch has been determined we evaluate C_0 with the following expression:

© Author(s) 2019

TABLE III. Circuit parameters for equivalent circuit models allowing only for the first resonance.

Model	Component	High-Q (Q = 100)	Low-Q (Q = 10)
BVD	C_0, F	$1.95\text{x}10^{-9}$	$1.94\text{x}10^{-9}$
	C_1, F	$4.77\text{x}10^{-10}$	$4.99\text{x}10^{-10}$
	L_1, H	$5.54\text{x}10^{-5}$	$5.42\text{x}10^{-5}$
	R_1, Ω	3.83	37.7
Sherrit	C_0', F	$1.95\text{x}10^{-9}/1.20°$	$1.95\text{x}10^{-9}/1.42°$
	C_1', F	$4.76\text{x}10^{-10}/2.69°$	$4.71\text{x}10^{-10}/9.59°$
	L_1', H	$5.55\text{x}10^{-5}/1.82°$	$5.98\text{x}10^{-5}/21.9°$

$$C_0' = \frac{A\varepsilon_{33}^S}{t\left(1-k_t^2\right)} - \left(C_1' + \cdots + C_N'\right) \tag{9}$$

The IEEE/ANSI standard on piezoelectricity[5] defines the parameters f_p and f_s as real values of the frequencies for maximum resistance and maximum conductance, respectively. Sherrit *et al.*[6] appear to be the first to treat f_p and f_s as complex variables to be compatible with lossy piezoelectric resonators and use this procedure to predict multiple resonances; in this case the analysis was for the radial mode instead of the thickness mode which we have studied.

Table IV gives the complex values of f_p and f_s that we calculated for the first 5 resonances using iteration with Eq. (1):

To avoid confusion, we have labeled the parameter f_p used by Sherrit et al.[3] as F_p in this paper. The parameter F_p in Eq. (1) is a function of the material parameters which is used in Eq. (1) to determine the impedance at any frequency. Notice that f_{p1} is not exactly equal to F_p, but rather f_{p1} must also be determined by the process that has just been defined and used to prepare Table V. This difference is more pronounced with the low-Q example.

Now that f_{pn} and f_{sn} have been determined in Table V, the components C_n' and L_n' in the proposed extension of the Sherrit model may be evaluated with Eqs. (10) and (11), and then C_0' may be determined with Eq. (9).

$$C_n' = \frac{A\varepsilon_{33}^S}{t\left(1-k_t^2\right)}\left[1-\left(\frac{f_{sn}'}{f_{pn}'}\right)^2\right] \quad \text{for n = 1 to N} \tag{10}$$

$$L_n' = \frac{1}{(2\pi f_{sn}')^2 C_n'} \quad \text{for n = 1 to N} \tag{11}$$

The admittance of the equivalent circuit may be calculated as follows:

$$Y(\omega) = j\omega C_0' + \frac{j\omega C_1'}{1-\omega^2 L_1' C_1'} + \frac{j\omega C_2'}{1-\omega^2 L_2' C_2'} + \cdots + \frac{j\omega C_N'}{1-\omega^2 L_N' C_N'} \tag{12}$$

$$\text{or } Y(\omega) = \frac{j\omega A\varepsilon_{33}^S}{t\left(1-k_t^2\right)} + \sum_{n=1}^{N} \frac{j\omega^3 L_n' C_n'^2}{1-\omega^2 L_n' C_n'} \tag{13}$$

We have used Eq. (13) to determine the impedance of our extension of the Sherrit model for the equivalent circuit because the modular nature of this equation makes it possible to determine the contribution for each branch separately and then these values may be combined to obtain the solution for various values of N. Figure 11 shows the impedance calculated for the equivalent circuit with N = 5 (circles) and using Eq. (1) for the analytical solution (solid lines).

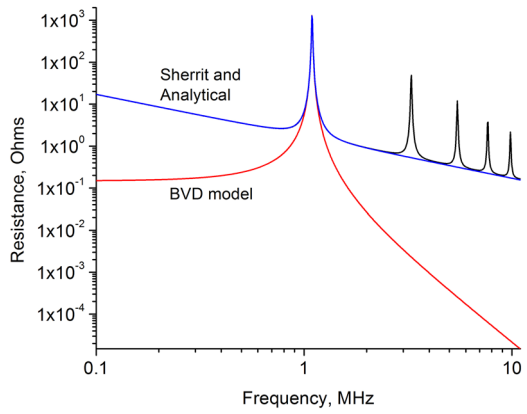

FIG. 9. Resistance calculated with the Sherrit and BVD equivalent circuits and the analytical solution for the high-Q example.

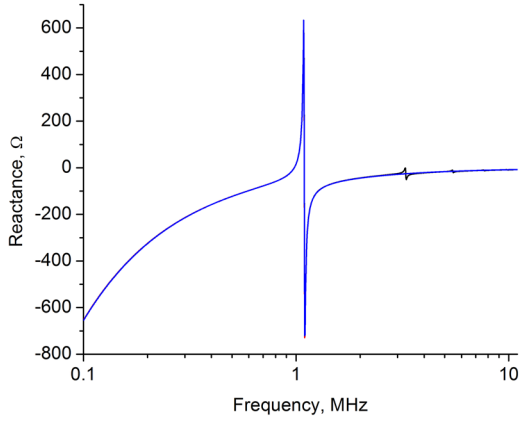

FIG. 10. Reactance calculated with the Sherrit and BVD equivalent circuits and the analytical solution for the high-Q example.

© Author(s) 2019

TABLE IV. Calculated values of f_p and f_s for the two examples.

	High-Q (Q = 100)		Low-Q (Q = 10)	
n	f_{pn}, MHz	f_{sn}, MHz	f_{pn}, MHz	f_{sn}, MHz
1	1.0924/0.2865°	0.9793/0.4331°	1.0950/2.8553°	0.9833/3.6506°
2	3.2771/0.2865°	3.2426/0.2987°	3.2851/2.8553°	3.2510/2.9221°
3	5.4618/0.2865°	5.4413/0.2908°	5.4752/2.8553°	5.4549/2.8789°
4	7.6465/0.2865°	7.6319/0.2887°	7.6653/2.8553°	7.6508/2.8673°
5	9.8312/0.2865°	9.8198/0.2878°	9.8554/2.8553°	9.8442/2.8625°

TABLE V. Calculated values of C_n and L_n in the extended equivalent circuits for the two examples.

	High-Q (Q = 100)		Low-Q (Q = 10)	
n	C_n, F	L_n, H	C_n, F	L_n, H
1	$4.76x10^{-10}$/-2.69°	$5.55x10^{-5}$/1.82°	$4.71x10^{-10}$/-9.60°	$5.56x10^{-5}$/2.29°
2	$5.06x10^{-11}$/-2.64°	$4.76x10^{-5}$/2.04°	$5.02x10^{-11}$/-9.32°	$4.78x10^{-5}$/3.48°
3	$1.82x10^{-11}$/-2.64°	$4.71x10^{-5}$/2.06°	$1.80x10^{-11}$/-9.31°	$4.73x10^{-5}$/3.55°
4	$9.26x10^{-12}$/-2.64°	$4.69x10^{-5}$/2.06°	$9.18x10^{-12}$/-9.30°	$4.71x10^{-5}$/3.57°
5	$5.60x10^{-12}$/-2.64°	$4.69x10^{-5}$/2.06°	$5.55x10^{-12}$/-9.30°	$4.71x10^{-5}$/3.58°

Solid circles and solid black lines are for the high-Q example and open circles with solid gray lines are for the analytical solution at the same set of frequencies with steps of 0.03 MHz. A linear frequency scale is used to provide greater detail at each resonance. Good agreement of these two methods is seen for both the high-Q and low-Q examples. We have only simulated the thickness mode, and acknowledge that, for this wide of a frequency range, other modes would also be present. Furthermore we have only included the effects of one of the thickness modes where three are possible as described by Balato.[13] Table V gives the values for C_n' and L_n' that were used in these calculations.

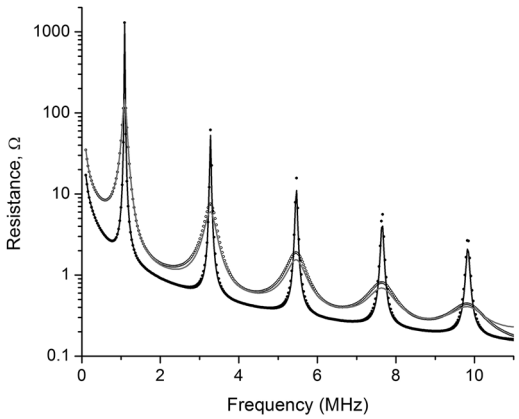

FIG. 11. Calculated resistive part of the impedance including the first 5 resonances for the high-Q and low-Q examples, where circular symbols represent calculations using Eq. (12) and solid lines for the analytical solutions using Eq. (1).

IV. CONCLUSIONS

1. The complex frequency for parallel resonance (f_p) is equal to an integer multiple of the parameter which we call F_p and need not be found by the general method of iteration.
2. The complex frequency for series resonance (f_s) must be determined by iteration since the real part of Y is bounded at this point in the complex frequency plane, which occurs because the imaginary part of Z is non-zero at that same point. However, simpler means have been determined for these iterations.
3. An equivalent circuit has been developed which accurately predicts the impedance from DC through the first five resonances, in agreement with the equation for the impedance, and may be extended for use over a greater frequency range.

ACKNOWLEDGMENTS

The author acknowledges helpful communications with Dr. Stewart Sherrit. This work began as part of an effort to develop an advanced scanning tunneling microscope which was supported by the Department of Energy under Award No. DE-SC0006339.

REFERENCES

[1] D. A. Berlincourt, D. R. Curran and H. Jaffe, "Piezoelectric and piezomagnetic materials and their function in transducers," in *Physical Acoustics–Principles and Methods*, vol. 1, part A, ed. W. P. Mason, New York, Academic, 1964, ch. 3, pp. 169–270.
[2] T. R. Meeker, "Thickness mode piezoelectric transducers," Ultrasonics **10**, 26–36 (1972).
[3] S. Sherrit, H. D. Wiederick, B. K. Mukherjee, and M. Sayer, "An accurate equivalent circuit for the unloaded piezoelectric vibrator in the thickness mode," J. Phys. D: Appl. Phys. **30**, 2354–2363 (1997).

© Author(s) 2019

[4]S. Sherrit and B. K. Mukherjee, "Characterization of piezoelectric materials for transducers," in *Dielectric and Ferroelectric Reviews*, eds. B. Srowthi and R. A. Dorey, Scarborough, Ontario, Canada, Research Signpost, 2012.
[5]1987, *IEE Standard on Piezoelectricity*, IEEE/ANSI-176.
[6]S. Sherrit, N. Gauthier, H. D. Wiederick, and B. K. Mukherjee, "Accurate evaluation of the real and imaginary material constants for a piezoelectric resonator in the radial mode," Ferroelectrics **119**, 17–32 (1991).
[7]S. Sherrit, H. D. Wiederick, and B. K. Mukherjee, "Non-iterative evaluation of the real and imaginary material constants of piezoelectric resonators," Ferroelectrics **134**, 111–119 (1992).
[8]S. Butterworth, "On electrically-maintained vibrations," Proc. Phys. Soc. London **27**, 420–424 (1915).
[9]K. S. Van Dyke, "The piezo-electric resonator and its equivalent network," Proc. IRE **16**, 742–764 (1928).
[10]A. Ballato, "Resonance in piezoelectric vibrators," Proc. IEEE **58**, 149–151 (1970).
[11]M. J. Guan and W. H. Liao, "On the equivalent circuit models of piezoelectric ceramics," Ferroelectrics **386**, 77–87 (2009).
[12]J. Kim, B. L. Grisso, J. K. Kim, D. S. Ha, and D. J. Inman, "Electrical modeling of piezoelectric ceramics for analysis and evaluation of sensory systems," in SAS 2008—IEEE Sensors Applications Symposium, 2008.
[13]A. Ballato, "Modeling piezoelectric and piezomagnetic devices and structures via equivalent networks," IEEE Trans. Ultrason. Ferroelectr. Freq. Control **48**, 1189–1240 (2001).

© Author(s) 2019